The FEBS Journal

FEBS PRESS science publishing by scientists

Overexpression of bromodomain factor 3 in *Trypanosoma cruzi* (*Tc*BDF3) affects differentiation of the parasite and protects it against bromodomain inhibitors

Victoria Lucia Alonso[1], Carla Ritagliati[2], Pamela Cribb[1,2], Julia Alejandra Cricco[1,2] and Esteban Carlos Serra[1,2]

1 Facultad de Ciencias Bioquímicas y Farmacéuticas, Universidad Nacional de Rosario, Argentina
2 Instituto de Biología Molecular y Celular de Rosario (IBR), CONICET, Rosario, Argentina

Keywords
acetylation; bromodomain; bromodomain inhibitor; p*Tc*INDEXGW; *Trypanosoma cruzi*

Correspondence
E. C. Serra, Instituto de Biología Molecular y Celular de Rosario (IBR), CONICET, Suipacha 590, 2000 Rosario, Argentina
Fax: +54 0341 4804598
Tel: +54 0341 4350661
E-mail: eserra@fbioyf.unr.edu.ar

(Received 24 October 2015, revised 16 February 2016, accepted 22 March 2016)

doi:10.1111/febs.13719

The bromodomain is the only protein domain known to bind acetylated lysine. In the last few years many bromodomain inhibitors have been developed in order to treat diseases such as cancer caused by aberrant acetylation of lysine residues. We have previously characterized *Trypanosoma cruzi* bromodomain factor 3 (*Tc*BDF3), a bromodomain with an atypical localization that binds acetylated α-tubulin. In the present work we show that parasites overexpressing *Tc*BDF3 exhibit altered differentiation patterns and are less susceptible to treatment with bromodomain inhibitors. We also demonstrate that recombinant *Tc*BDF3 is able to bind to these inhibitors *in vitro* in a concentration-dependant manner. In parallel, the overexpression of a mutated version of *Tc*BDF3 negatively affects growth of epimastigotes. Recent results, including the ones presented here, suggest that bromodomain inhibitors can be conceived as a new type of anti-parasitic drug against trypanosomiasis.

Introduction

Trypanosoma cruzi is a protozoan parasite and the causative agent of Chagas disease. This endemic disease is an important public health issue in Latin America currently affecting an estimated 8 million people in 21 countries, with roughly 50 000 new cases per year and spreading continuously to many non-endemic regions via human migration. The two registered drugs for Chagas disease treatment were introduced in the 1960s (nifurtimox, Bayer) and 1970s (benznidazole, Roche). Both drugs are effective in newborns and in the acute phase but their use during the chronic phase is still controversial and requires prolonged treatment that has frequent side-effects [1].

Trypanosoma cruzi has a complex life cycle with two intermediate hosts, a triatomine insect and a mammalian vertebrate, where it invades almost all nucleated cells. Several developmental stages are found in the hosts: amastigotes and bloodstream trypomastigotes are present in the mammalian vertebrates, whereas epimastigotes and the infective metacyclic trypomastigotes are present in the insect vector [2]. The differentiation event from epimastigotes to metacyclic trypomastigotes, occurring inside the insect, is called metacyclogenesis. This process can be induced *in vitro* using artificial media [3].

Trypanosomatids have a simple but precisely ordered cytoskeleton, primarily made of stable microtubules (MTs) [4]. MTs constitute four substructures in trypanosomatids: the mitotic spindle, the flagellar axoneme, the basal body of the flagellum and, most importantly, the subpellicular corset. This corset is made exclusively of a dense network of MTs

Abbreviations
BDF, bromodomain factor; BRD, bromodomain; GAPDH, glyceraldehyde 3-phosphate dehydrogenase; HA, haemagglutinin; KAc, acetylated lysine; MT, microtubule; PCAF, p300/CBP-associated factor; TAT, tubulin acetyltransferase; Tet, tetracycline.

cross-linked to each other and to the plasma membrane, forming a helical pattern along the long axis of the cell (reviewed in [5]). It is responsible for shaping the cell and plays a major role in events such as positioning of organelles, mitosis and cytokinesis.

Acetylated α-tubulin is found to be predominant in the subpellicular and axonemal microtubules and in the flagella of *T. cruzi* and *Trypanosoma brucei* [6,7]. This post-translational modification is also present in the ephemeral microtubules of the mitotic spindle of *T. brucei* [4]. In the cytoplasm, tubulin is the major target of acetylation and the canonical site for tubulin acetylation is lysine (K) 40 of α-tubulin [8], which unlike tyrosination and glutamylation sites, is located on the MT luminal surface [9]. How the acetytransferases and deacetylases gain access to K40 is unclear, but recent studies suggest that human tubulin acetyltransferase (αTAT) efficiently scans MTs bidirectionally within the lumen by surface diffusion, acetylating K40 stochastically [10].

The bromodomain is a conserved structural module present mainly in nuclear proteins that recognize acetylated lysines (KAc) on histones and non-histone proteins. Histone acetyltransferases associate with transcriptional cofactors that contain bromodomains, bind acetylated histones and allow the epigenetic spread of this modification in the chromatin [11]. Although no such cofactors that would 'spread' tubulin acetylation inside microtubules have been discovered, acetylation could alter the binding of proteins accessing the luminal surface of the microtubule. The identity of these proteins is unknown, but the presence of luminal particles has been confirmed for many cell types [12–14].

Bromodomains comprise ~ 110 amino acids that form a characteristic antiparallel four-helix bundle containing helices αZ, αA, αB and αC. The KAc binds to a well-defined hydrophobic pocket at one end of the helical bundle. Recent studies using small-molecule inhibitors targeting bromodomain proteins highlight the functional importance of bromodomain–KAc binding as a key mechanism in orchestrating molecular interactions and regulation of chromatin biology and gene transcription. They report that the modulation of these interactions with small-molecule chemicals offers new therapeutic opportunities for a wide array of human diseases including cancer and inflammation (reviewed in Ref. [15]).

We have previously characterized bromodomain factor 3 from *T. cruzi* (*Tc*BDF3), the first reported exclusively non-nuclear bromodomain-containing protein. *Tc*BDF3 is expressed in all life cycle stages and interacts with acetylated α-tubulin, the major component of the flagellar and subpellicular microtubules. In both metacyclic and bloodstream trypomastigotes, *Tc*BDF3 was found to be concentrated in the flagellum and the flagellar pocket region [16]. *Tc*BDF3 seems to have a different function from its orthologue in *T. brucei*, which was very recently reported to be a nuclear protein involved in regulating the fate of the blood-stream form [17].

In the present study we used a tetracycline-inducible vector (p*Tc*INDEXGW) [18] to overexpress *Tc*BDF3 and a double mutant version in *T. cruzi*. The transfected lines show altered differentiation patterns and are less susceptible to the bromodomain inhibitors I-BET151 [19] and JQ1(+) [20]. We also demonstrated that recombinant *Tc*BDF3 is able to bind to these inhibitors *in vitro* in a concentration-dependant manner.

Results

Inducible expression of a mutant *Tc*BDF3 shows a dominant negative effect over epimastigote growth

A double mutant version of *Tc*BDF3 (hereafter, *Tc*BDF3m) was constructed changing Y123 and L130 for A based on sequence alignments with human p300/CBP-associated factor (PCAF) bromodomain (Fig. 1 A). Homologue mutations in PCAF were found to disrupt the bromodomain acetyl-lysine binding capacity without altering its structure [21]. We have previously characterized the *in vitro* interaction between recombinant *Tc*BDF3 and acetylated α-tubulin synthetic peptides [16]. Using the same methodology we tested if recombinant *Tc*BDF3m was able to bind the acetylated tubulin peptide (Fig. 1B). We observed by slot-blot assays that the change of Y123 and L130 for A impairs the correct binding of the acetylated substrate. The correct folding of the recombinant proteins was assessed by circular dicroism spectroscopy (Fig. 1C).

We overexpressed haemagglutinin (HA)-tagged *Tc*BDF3 and *Tc*BDF3m in *Trypanosoma cruzi* epimastigotes using the tetracycline-inducible vector p*Tc*INDEXGW [18,22]. The induction of the expression by tetracycline was tested by western blot assays (Fig. 2A) and immunofluorescence microscopy (Fig. 2B), using rat monoclonal anti-HA and rabbit polyclonal anti-*Tc*BDF3 antibodies. We quantified the bands from the western blot and determined that the exogenous protein overexpression is ~ 20-fold over the endogenous protein (Fig. 2A, right panel). Overexpression was also confirmed by quantitative RT-PCR showing a 10-fold increase of *Tc*BDF3 mRNA in the

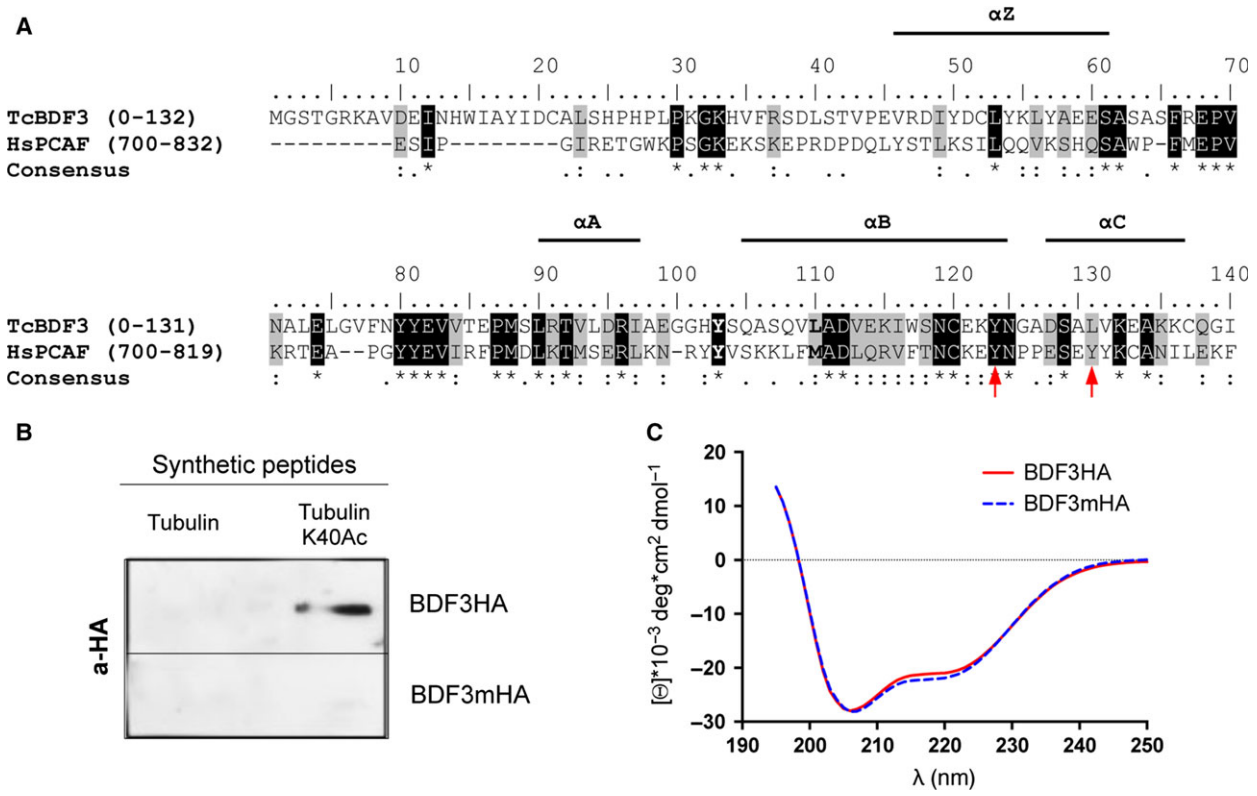

Fig. 1. The double mutant *Tc*BDF3 m is not able to interact with acetylated α-tubulin *in vitro*. (A) Sequence alignment of *Tc*BDF3 and human PCAF bromodomains using CLUSTALX2.1 manually edited to highlight conserved (grey background) and identical (black background) residues based on BLOSUM 62 substitution matrix data. α-Helix regions of the bromodomain are marked. The amino acids mutates are indicated with red arrows. (B) Slot far-western blot assay: non-acetylated α-tubulin (Tubulin) and acetylated α-tubulin (Tubulin K40Ac) peptides were blotted onto a nitrocellulose membrane and incubated with haemagglutinin (HA) -tagged recombinant BDF3HA or BDF3mHA. Bound recombinant proteins were detected with anti-HA antibodies (a-HA). (C) Secondary structure of the recombinant proteins measured by circular dicroism spectroscopy.

induced lines (Fig. 2C). Even though overexpression levels are high, the localization pattern in epimastigotes of both wild-type and double mutant *Tc*BDF3 resembles the one observed for the endogenous protein [16]. We observed that the exogenous proteins localize in the cell body excluded from the nucleus and that the flagellar pocket region is more deeply marked (Fig. 2B).

Then, we monitored the effect of overexpression on the epimastigote's growth after induction with tetracycline (Fig. 2D). The Dm28*c* p*Tc*INDEXGW-*Tc*BDF3HA cell line grew at similar rates in the absence and presence of tetracycline, but parasites harbouring *Tc*BDF3mHA showed a delay in their growth rate when induced, behaving as a dominant negative mutant. We also observed morphological changes in these parasites; almost 20% of them were aflagellate cells, determined by direct microscopy of Giemsa-stained smears (18.9 ± 0.89% were aflagellate forms when Dm28c p*Tc*INDEXGW-*Tc*BDF3HA was induced with tetracycline and 3.81 ± 0.54% were aflagellate without tetracycline). No morphological changes were observed when the expression of *Tc*BDF3HA was induced. We also determined the presence of *Tc*BDF3HA (Fig. 3A) and *Tc*BDF3mHA (Fig. 3B) in isolated cytoskeletal and flagellar complexes of epimastigotes and we observed co-localization with the endogenous protein using anti-HA and anti-*Tc*BDF3 antibodies.

Overexpression of *Tc*BDF3HA and *Tc*BDF3mHA alters metacyclogenesis and infection rates

We have previously reported that *Tc*BDF3 changes its localization during metacyclogenesis (concentrating in the flagellum of trypomastigotes) and binds acetylated α-tubulin in the cytoskeleton and flagella. Because cytoskeletal rearrangements are important during metacyclogenesis and infection [23], we decided to

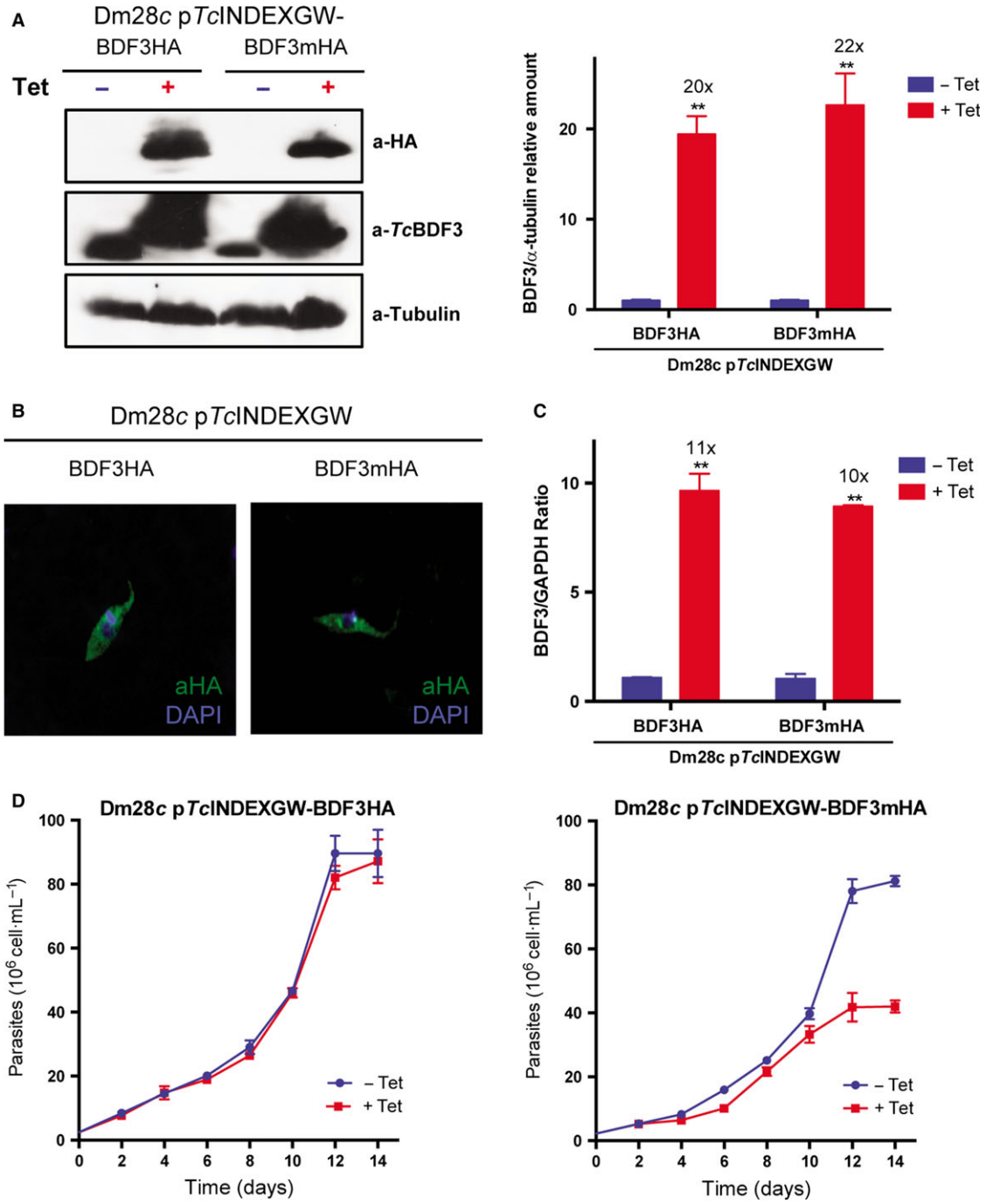

Fig. 2. Overexpression of *Tc*BDF3mHA alters epimastigotes' growth. (A) Equal amounts of parasite total lysate from Dm28c p*Tc*INDEXGW-BDF3HA and p*Tc*INDEXGW-BDF3mHA in the absence (–) or presence (+) of 0.25 μg·mL^{-1} tetracycline (Tet) for 48 h were loaded on SDS/PAGE followed by western blot analysis using rat anti-HA monoclonal antibodies (a-HA), mouse anti-tubulin (a-Tubulin) and purified rabbit polyclonal antibodies against *Tc*BDF3 (a-*Tc*BDF3). The intensity of the *Tc*BDF3 bands was quantified from three independent experiments and normalized to α-tubulin intensity. The bar graph on the right represents the mean ± SEM of the relative intensity of the bands; $^{**}P < 0.005$ (unpaired, two-tailed Student's *t* test). (B) Immunofluorescence microscopy of induced (0.25 μg·mL^{-1} tetracycline, 24 h) parasites using rat anti-HA and FITC-conjugated anti-rat antibodies (green). DNA was stained with DAPI (blue). (C) Quantitative PCR of *Tc*BDF3 mRNA in the uninduced (−Tet) and induced (+Tet) parasites. (D) Growth curves of epimastigotes transfected with p*Tc*INDEXGW-BDF3HA and -BDF3mHA in the absence (blue) or presence (red) of 0.5 μg·mL^{-1} tetracycline (which was re-added every 5 days) counted every 2 days during 14 days. Results are representative of three independent experiments.

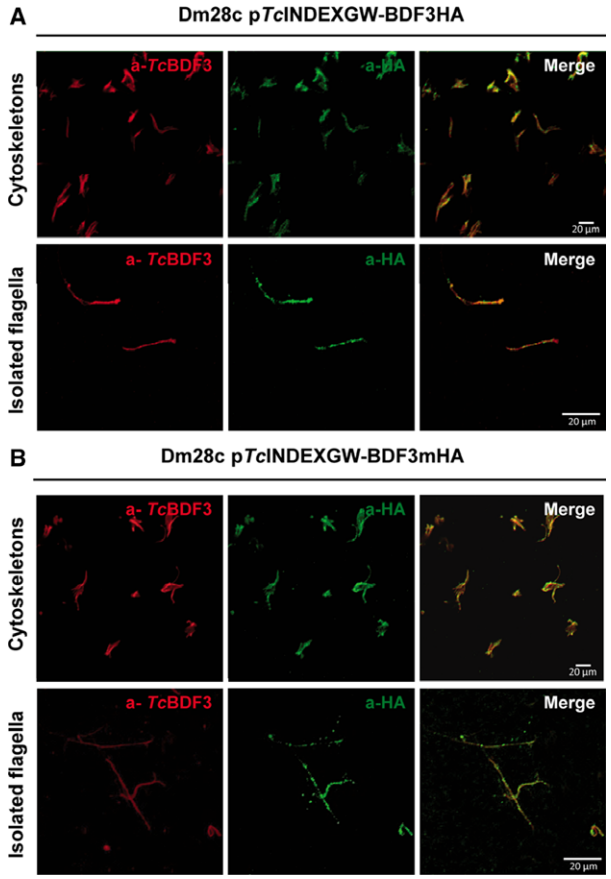

Fig. 3. *Tc*BDF3HA and *Tc*BDF3mHA are detected in the cytoskeletons and isolated flagella of epimastigotes. Immunofluorescence assays of isolated cytoskeletons and flagellar complex using purified rabbit anti-*Tc*BDF3 and monoclonal rat anti-HA antibodies of (A) Dm28c p*Tc*INDEXGW-BDF3HA and (B) Dm28c p*Tc*INDEXGW-BDF3mHA. Anti-rabbit IgG conjugated to Cy3 and anti-rat IgG conjugated to fluorescein were used as secondary antibodies.

quantify the differentiation and infection rates in parasites overexpressing the wild-type and the double mutant version of *Tc*BDF3. We verified the inducible expression of the exogenous proteins by western blot in trypomastigote (T) and amatigote (A) total extracts (Fig. 4A). *In vitro* metacyclic trypomastigotes were produced from transgenic epimastigotes using TAU medium, in the absence (−Tet) or presence (+Tet) of tetracycline for 72 h (Fig. 4B). Both transgenic lines showed a decrease in the percentage of metacyclic trypomastigotes obtained; however, this effect was more pronounced when *Tc*BDF3mHA was overexpressed.

To study the role of *Tc*BDF3 expression in the replicative form present inside the mammalian host, we performed *in vitro* infections. We previously infected Vero cells with Dm28*c* wild-type parasites to rule out any undesired effect of the tetracycline treatment. Indeed, there was no significant difference in the infectivity rate nor in the number of amastigotes per cell (data not shown). Then, Dm28*c* p*Tc*INDEXGW-BDF3HA and BDF3mHA trypomastigotes were preincubated in the absence or presence of tetracycline (0.25 $\mu g \cdot mL^{-1}$) and used to infect Vero cells at a ratio of 10 parasites per cell. After 6 h of infection at 37 °C, the free trypomastigotes were washed out and replaced by complete medium alone or with tetracycline (0.25 $\mu g \cdot mL^{-1}$) for 2 days. To analyse the effect of *Tc*BDF3 and *Tc*BDF3m overexpression on the infectivity rate of trypomastigotes, we focused on the condition in which the expression was induced only in the trypomastigote stage during infection (+Tet/−Tet) (Fig. 4C). While overexpression of *Tc*BDF3 diminished the infectivity rate of trypomastigotes, overexpression of *Tc*BDF3m slightly increased it (+Tet/−Tet vs −Tet/−Tet). To test the effect of *Tc*BDF3 and *Tc*BDF3m overexpression on the proliferation of intracellular amastigotes (Fig. 4D), we only added tetracycline after the infection, when the trypomastigotes were washed out, for 48 h post-infection (−Tet/+Tet). The number of amastigotes per infected cell slightly increased only when the double mutant was overexpressed (−Tet/+Tet vs −Tet/−Tet). Furthermore, the cells infected with the Dm28*c* p*Tc*INDEXGW-BDF3mHA-induced line released more trypomastigotes at day 6 post-infection (Fig. 4E).

Several human bromodomain inhibitors affect epimastigotes' growth

Bromodomain inhibitors are very useful tools to study the mechanism of action of this protein module. Therefore, we tested if different bromodomain inhibitors had any effect over *Trypanosoma cruzi*. We purchased six bromodomain inhibitors (Table 1) from ApexBio and we also tested I-BET151 (provided by GlaxoSmithKline). We calculated the IC_{50} values of these small molecules by counting epimastigotes 72 h after treatment. Two of these compounds, JQ1(+) and I-BET151, had lower IC_{50} values than benznidazole (Roche), the current drug for Chagas' disease treatment (Table 1).

Recombinant *Tc*BDF3 interacts with bromodomain inhibitors

Bromodomain inhibitors JQ1(+) and I-BET151 have preference for bromodomains of the human BET family (BRD2, BRD3, BRD4 and BRDT). Both inhibitors engage the bromodomain pocket in a manner that is

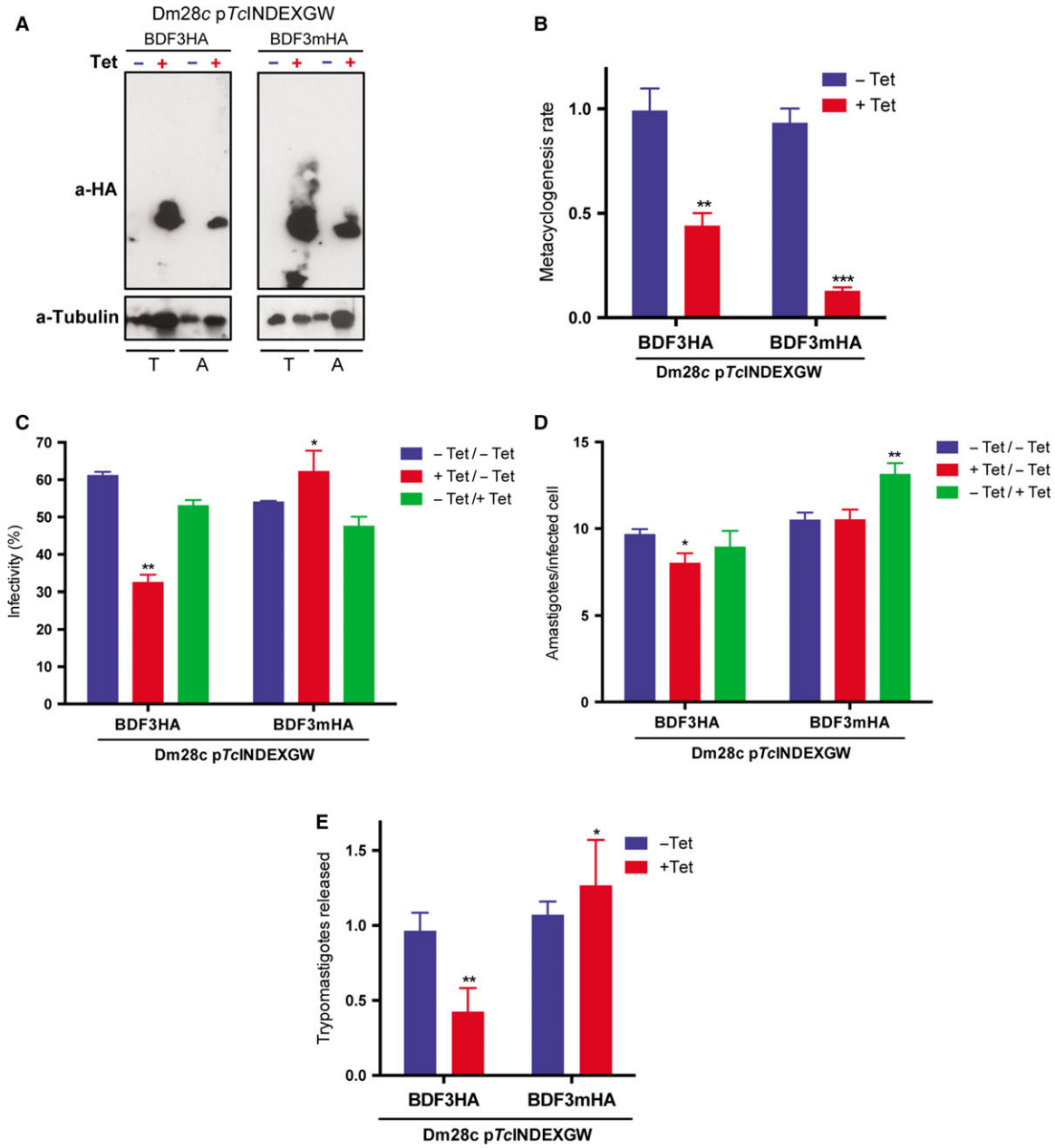

Fig. 4. Overexpression of *Tc*BDF3HA and *Tc*BDF3mHA alters metacyclogenesis and infection rates. (A) Equal amounts of trypomastigote (T) and amastigote (A) total lysates from Dm28c p*Tc*INDEXGW-BDF3HA and p*Tc*INDEXGW-BDF3mHA in the absence (–) or presence (+) of 0.25 μg·mL^{-1} tetracycline for 48 h were loaded on SDS/PAGE followed by western blot analysis using rat anti-HA monoclonal antibodies (a-HA) and mouse anti-tubulin (a-Tubulin). (B) *In vitro* metacyclogenesis using TAU medium of Dm28c p*Tc*INDEXGW-BDF3HA and BDF3mHA uninduced (–Tet) or induced (+Tet) with 0.5 μg·mL^{-1} tetracycline for 72 h. The bar graph represents the mean ± SEM from three independent experiments; $^{**}P < 0.005$ and $^{***}P < 0.001$ (unpaired, two-tailed Student's *t* test). (C,D) Vero cell infection. The infection and the post-infection incubation were performed in the absence or presence of 0.25 μg·mL^{-1} tetracycline: –Tet/–Tet, Tet was never added to the medium; +Tet/–Tet, trypomastigotes were pretreated with Tet for 3 h prior to infection, and Tet was added during the infection but not after; –Tet/+Tet, trypomastigotes were not induced, and Tet was only added for 48 h post-infection. The percentage of infected cells (C) and the number of amastigotes per cell (D) were determined by counting Giemsa-stained slides using a light microscope. Results are expressed as means ± SEM of triplicates, and represent one of three independent experiments performed. Each condition was analysed by unpaired two-tailed Student's *t* test with the control (–/–): $^{*}P < 0.05$, $^{**}P < 0.005$. (E) Fraction of trypomastigotes released 6 days post-infection of Dm28c p*Tc*INDEXGW-BDF3HA and BDF3mHA uninduced (–Tet) or induced (+Tet) with 0.5 μg·mL^{-1} tetracycline. The bar graph represents the mean ± SEM from three independent experiments; $^{*}P < 0.05$ and $^{**}P < 0.005$ (unpaired, two-tailed Student's *t* test).

Table 1. IC_{50} values of bromodomain inhibitors on *Trypanosoma cruzi* epimatigotes.

	I-BET151	JQ1(+)	JQ1(−)	PFI-1	RVX-208	SGC-CBP30	Bromosporine	BZN[a]
IC_{50} (μM)	6.35	7.137	> 50	> 50	> 50	25.72	> 50	9.87

[a] Benznidazole (reference drug use for Chagas disease treatment).

competitive with the acetylated substrate, causing the displacement of all four BET proteins from chromatin in cells upon exposure to these compounds. These inhibitors also have suitable pharmacokinetics for *in vivo* application, which has enabled a rapid evaluation of their therapeutic activity in various disease models [19,20,24,25].

We considered the possibility that these inhibitors might bind to recombinant *Tc*BDF3. We tested this hypothesis measuring the changes in the intrinsic fluorescence of *Tc*BDF3 upon exposure to JQ1(+) and I-BET151. Proteins are considered to have intrinsic fluorescence due to the presence of aromatic amino acids, mainly tryptophan (W). *Tc*BDF3 has two W, one located inside the hydrophobic pocket of the bromodomain (W117) and the other in the N-terminal region (W15). Figure 5 shows the quenching spectra of solutions containing a fixed concentration of *Tc*BDF3HA and increasing concentrations of each bromodomain inhibitor. The fluorescence intensities were corrected taking into account the inner filter effect as described in 'Materials and methods'. When increasing amounts of I-BET151 (Fig. 5A) and JQ1(+) (Fig. 5B) were added, we observed that the

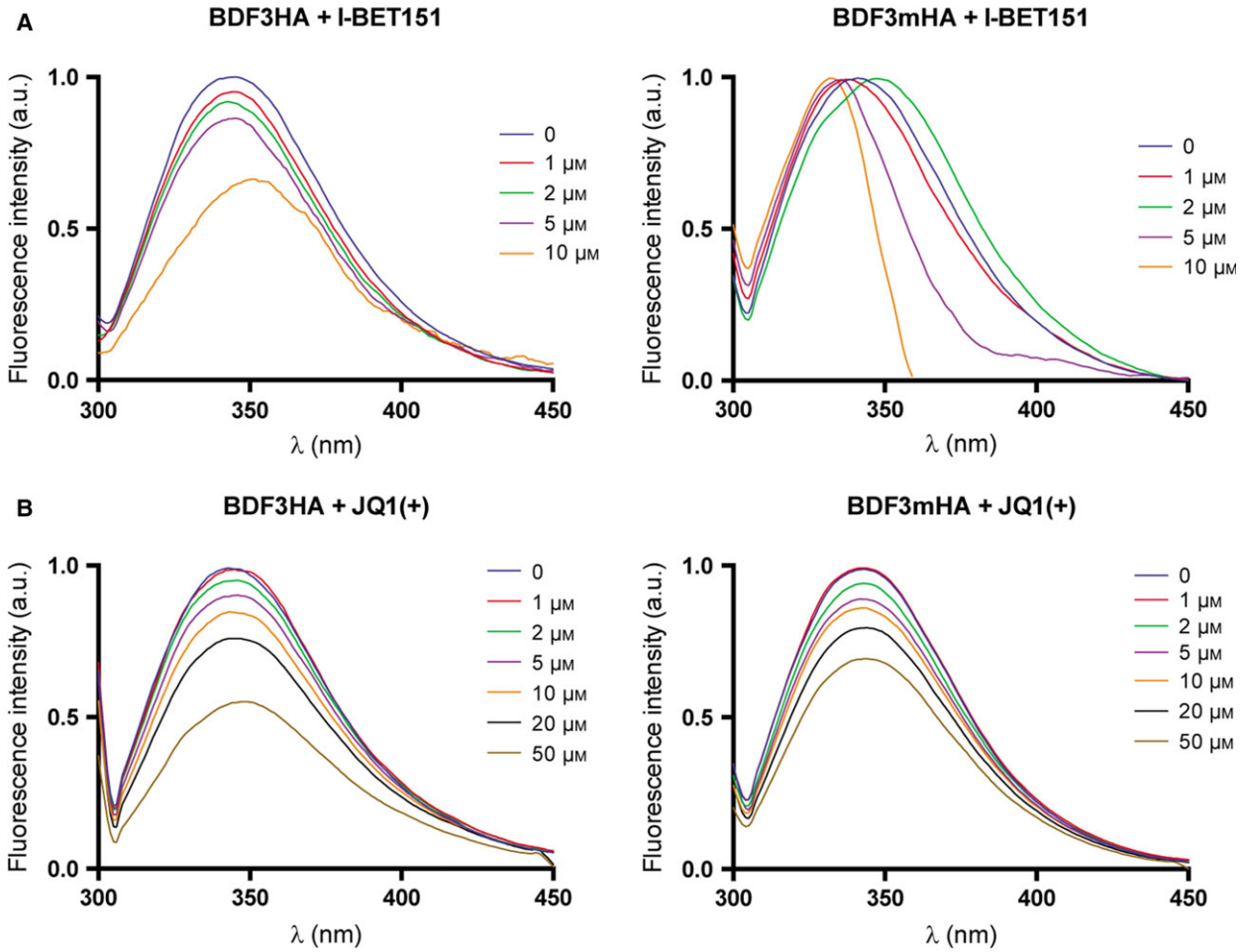

Fig. 5. Bromodomain inhibitors interact with recombinant *Tc*BDF3HA and *Tc*BDF3mHA. Fluorescence spectra of *Tc*BDF3HA and *Tc*BDF3mHA (5 μM) with an increasing amount of I-BET151 (A) and JQ1(+) (B). λ_{ex} = 295 nm.

fluorescence intensity of *Tc*BDF3 decreased regularly. For I-BET151, at higher concentrations this decrease was associated with a slight emission wavelength shift. The shift in the emission maximum towards longer wavelength suggests a decreased hydrophobicity in the microenvironment of the protein fluorophores upon interaction with I-BET151. These results indicate that both bromodomain inhibitors interact with *Tc*BDF3 and quench its intrinsic fluorescence, but not necessarily by the same binding mechanism.

The fluorescence quenching data were analysed by the Stern–Volmer equation: $F_0/F = 1 + K_{sv}[Q]$, where F_0 and F are the fluorescence intensities of *Tc*BDF3HA in the absence and presence of the bromodomain inhibitors; K_{sv} is the Stern–Volmer quenching constant, which is a measure of the quenching efficiency; and [Q] is the concentration of I-BET151 or JQ1(+). The plots F_0/F vs [Q] showed a negative deviation (towards the x-axis). This is a characteristic feature of a population of two fluorophores, one of which is not accessible to the quencher, consistent with the presence of only one W in the acetyl-lysine binding pocket, as predicted by the analysis of the 3D modelled structure of *Tc*BDF3. In the case of fluorescing tryptophans in structured proteins, the W residues are buried within the protein and as such give rise to heterogeneous quenching. Some residues that are involved in the binding site of a ligand acting as a quencher are readily available to quenching while others that are not involved in binding may not be quenched at all. The data were further examined using the modified Stern–Volmer equation: $F_0/(F_0 - F) = 1/f_a + 1/(f_a K'_{sv}[Q])$, where F_0 and F are the corrected fluorescence intensity of *Tc*BDF3 in the absence and presence of the inhibitors at concentration [Q], f_a is the fraction of accessible fluorescence and K'_{sv} is the effective quenching constant. From the plots of $F_0/(F_0 - F)$ vs $1/[Q]$, the values of f_a and K_{sv} were obtained (Table 2). If the quenching process arises from binding between the fluorophore and the quencher, then regardless of the population of inaccessible fluorophores, a plot of $F_0/(F_0 - F)$ vs $1/[Q]$ is linear. The f_a values indicate that for both I-BET151 and JQ1(+) half of the fluorescence is accessible to the quencher, consistent with two W populations present in *Tc*BDF3.

The values of the association or binding constant (K_a) for the bromodomain inhibitor–*Tc*BDF3 interaction (Table 2) for these inhibitors were determined from the double-logarithmic plots of log $(F_0 - F)/F$ vs log[Q]. As expected, these plots indicate that there is only one binding site for the inhibitors in *Tc*BDF3. The dissociation constant (K_d) is described as the reciprocal of K_a (Table 2). The K_d values obtained for I-BET151 and JQ1(+) are at least one order of magnitude higher than those reported for human bromodomains (between 0.05 and 0.2 μM for JQ1(+) and between 0.1 and 0.8 μM for I-BET151 (http://pubchem.ncbi.nlm.nih.gov). These results also suggest that the binding mode of both inhibitors with *Tc*BDF3 might be different from the human bromodomains, as was recently showed for Bdf2 from *T. brucei* and I-BET151 [17] (see 'Discussion').

Table 2. Values of K_{sv}, fraction of accessibility of fluorophores to the quencher calculated from the modified Stern–Volmer (f_a), association constant (K_a) and number of binding sites (n) calculated from the double-logaritmic plots.

	Modified Stern–Volmer			Double-logaritmic			
	K_{sv} (μM^{-1})	f_a	R^2	K_a (μM^{-1})	n	R^2	K_d (μM)
I-BET151	0.037	0.486	0.86	0.046	0.86	0.98	21.7
JQ1(+)	0.019	0.575	0.84	0.026	0.92	0.97	38.4

When the same experiments were performed with recombinant *Tc*BDF3m we observed a different behaviour for the two inhibitors (Fig. 5A,B, right panel). I-BET151 did not modify the fluorescence emission maxima of the protein whereas JQ1(+) decreased it, but to a lower extent than the wild-type protein.

Epimastigotes overexpressing *Tc*BDF3 are less susceptible to bromodomain inhibitors

We evaluated if bromodomain-overexpressing lines were less sensitive to the inhibitors. Epimastigotes overexpressing *Tc*BDF3 and *Tc*BDF3m were treated with JQ1(+) and I-BET151, in the absence (−Tet) and presence (+Tet) of tetracycline. As seen in Fig. 6A, overexpression of *Tc*BDF3 rescued epimastigotes from the growth inhibition of I-BET151 and JQ1(+) completely. As expected, when we treated the lines overexpressing *Tc*BDFm with I-BET151 we did not observe a growth recovery, indicating that the mutated amino acids are also implicated in the binding of this inhibitor. On the contrary, a growth recovery was observed in the presence of JQ1(+), suggesting that *Tc*BDF3m retains, at least in part, its ability to bind to this compound. These results are consistent with the fluorescence spectra obtained for *Tc*BDF3m with JQ1(+).

Also, we determined if recombinant *Tc*BDF3 was able to bind to the acetylated α-tubulin peptide in the presence of I-BET151 and JQ1(+) (Fig. 6B). In both cases the interaction was impaired, suggesting that the

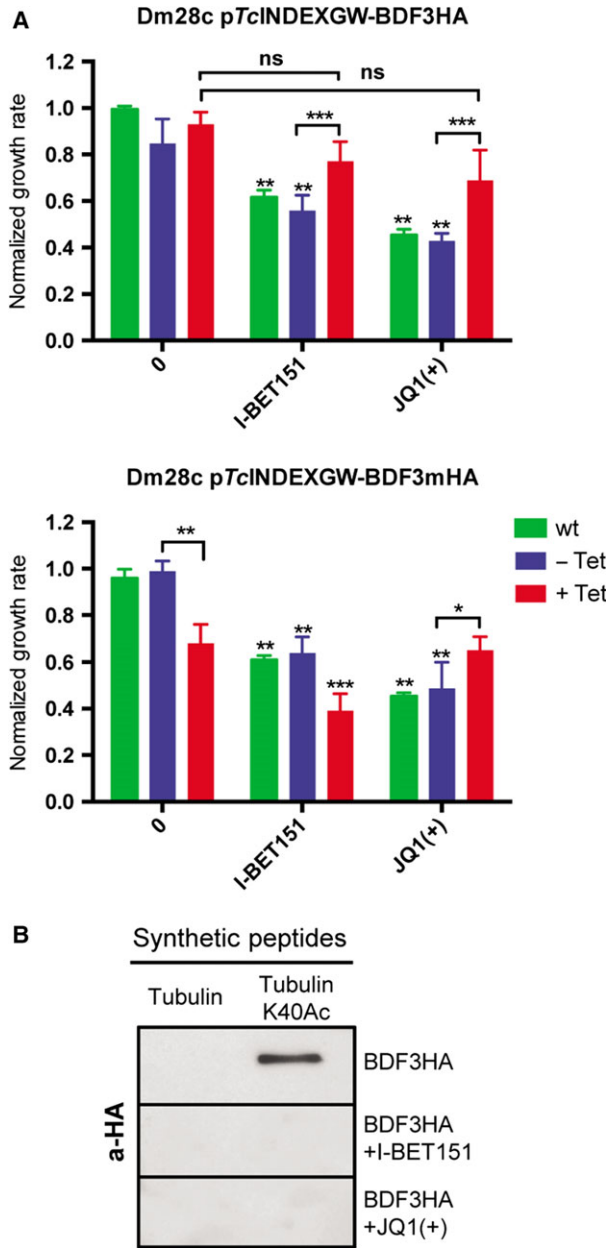

Fig. 6. Epimastigotes overexpressing *Tc*BDF3HA and *Tc*BDF3mHA are less susceptible to bromodomain inhibitors. (A) Dm28c wild-type (green bars) and uninduced (blue bars) and induced (red bars) epimastigotes of both transfected lines (Dm28c p*Tc*INDEXGW-BDF3HA and BDF3mHA) were treated with two bromodomain inhibitors with concentrations above their IC_{50} values (10 μM I-BET151 and JQ1(+)). The experiment was performed in triplicate and cell growth was determined after 72 h of culture by counting viable forms. The values obtained were normalized to the wild-type growth without inhibitors. The growth rate of each transfected line with inhibitors was compared with the corresponding untreated one. We also compared the viability of the uninduced and induced overexpressing lines with the wild-type, and the induced transfected lines with the wild-type (in the case of Dm28c p*Tc*INDEXGW-BDF3HA). The bar graph represents the mean ± SEM; $*P < 0.05$, $**P < 0.005$, $***P < 0.001$ (unpaired, two-tailed Student's *t* test). (B) Slot far-western blot assay: non-acetylated α-tubulin (Tubulin) and acetylated α-tubulin (Tubulin K40Ac) peptides were blotted onto a nitrocellulose membrane and incubated with HA-tagged recombinant BDF3HA in the absence or presence of 10 μM I-BET151 or JQ1(+). Bound recombinant protein was detected with anti-HA antibodies (a-HA).

compounds interact with the acetylated-lysine binding pocket of *Tc*BDF3.

As a control, we also evaluated the effect of JQ1(−), the enantiomer of JQ1(+), which showed no significant binding to human bromodomains [20]. This inhibitor did not show any effect over the wild-type (Fig. 7A), nor the overexpressing *Tc*BDF3 parasites, using the same concentration as JQ1(+) (Fig. 7B). Furthermore, this inhibitor did not affect the fluorescence spectra of *Tc*BDF3 (Fig. 7C).

Discussion

We have previously described the atypical cytoplasmic bromodomain-containing protein *Tc*BDF3. In epimastigotes *Tc*BDF3 binds acetylated α-tubulin from both the subpellicular network and the flagellar axoneme, while in trypomastigotes it is located only in the axoneme [16]. We determined that in all life cycle stages *Tc*BDF3 was located outside the nucleus and although we cannot exclude its interaction with other cytoplasmic proteins, the concentration of *Tc*BDF3 in the flagellum of trypomastigotes during metacyclogenesis suggests its involvement in this differentiation process. Given the difficulty of generating deletion mutants and the absence of RNA interference machinery in *T. cruzi*, we decided to use a dominant negative mutant strategy to prove this hypothesis. With this objective, we constructed a mutated version of *Tc*BDF3 (*Tc*BDF3mHA), which we overexpressed in an inducible manner in *T. cruzi* Dm28*c* strain. *Tc*BDF3mHA lacks the ability to bind acetylated α-tubulin peptides. In our present work we determined that the correct function of *Tc*BDF3 is necessary for epimastigote growth, since *Tc*BDF3mHA overexpression impairs it. The presence of aflagellate parasites (when *Tc*BDF3mHA was overexpressed) suggests the involvement of *Tc*BDF3 in the genesis and maintenance of this cellular structure in epimastigotes. We have previously shown that a truncated version of *Tc*BDF3 (bearing only the bromodomain) is localized outside of the cytoskeleton; however the double mutant version of *Tc*BDF3 is localized in the microtubules, as is the wild-type protein. This suggests that

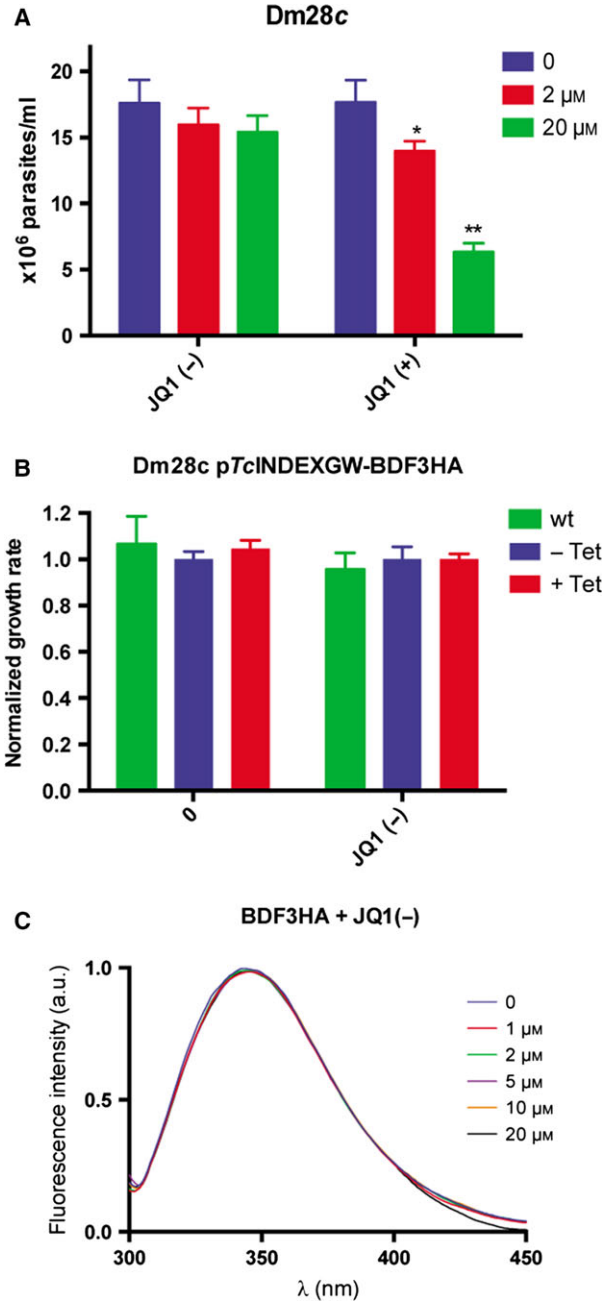

Fig. 7. JQ1(–) bromodomain inhibitor does not affect epimastigotes' growth nor interact with recombinant *Tc*BDF3. (A) Number of parasites per millilitre of wild-type Dm28c in the presence of increasing concentrations of JQ1(–) and JQ1(+) after 72 h of treatment. (B) Wild-type Dm28c strain (green bars) and uninduced (blue bars) and induced (red bars) epimastigotes of Dm28c p*Tc*INDEXGW-BDF3HA were treated with 10 μM JQ1(–). The experiment was performed in triplicate and cell growth was determined after 72 h of culture by counting viable forms. The values obtained were normalized to the wild-type growth without inhibitors. The growth rate of the transfected line with JQ1(–) was compared to the corresponding untreated condition (non-significant). We also compared the viability of the uninduced and induced overexpressing line with the wild-type (non-significant). The bar graph represents the mean ± SEM (unpaired, two-tailed Student's *t* test). (C) Fluorescence spectra of *Tc*BDF3HA (5 μM) with increasing amounts of JQ1(–). λ_{ex} = 295 nm.

targeting of *Tc*BDF3 to microtubules is independent of its ability to bind acetyl-lysines, and mediated by other protein(s) that interact with its C-terminal region. The importance of *Tc*BDF3 in the metacyclogenesis process is also clearly shown by the fact that not only does the expression of *Tc*BDF3m diminish the differentiation rate from epimastigotes to trypomastigotes but also the overexpression of the wild-type protein has a similar effect, suggesting that in this case *Tc*BDF3 function might be independent of its acetyl-lysine binding capacity. A possible explanation for this observation is that a tightly regulated amount of *Tc*BDF3 could be needed for an efficient metacyclogenesis, through a protein complex with other (yet unknown) proteins, and that overexpressing the wild-type bromodomain could modify the equilibrium of the complex, perturbing the differentiation.

In the other life cycle stages, overexpression of the wild-type and the mutated protein has different effects and suggests that *Tc*BDF3 affects the differentiation pathways by different mechanisms. Overexpression of *Tc*BDF3 in trypomastigotes decreases their infectivity, whereas *Tc*BDF3m increases it. The development of intracellular amastigotes also improved when *Tc*BDF3mHA was overexpressed, in correlation with an increased number of trypomastigotes released when cells exploded. In contrast, overexpression of *Tc*BDF3HA seems not to affect amastigote growth but it appears to be necessary for the development of the trypomastigote flagella during differentiation from amastigotes.

Although tubulin acetylation is a widespread modification present in all eukaryotic cells, its precise function in cytoskeleton dynamics has not been completely elucidated yet. In most eukaryotes, the number of acetytrasferases and deacetylases is limited and most of them have different functions when located in different cellular compartments. Participation of tubulin acetylation in neuronal differentiation was proposed many years ago [26,27]. However, functional association of acetylating (ELP3) and deacetylating (HDAC6) enzymes in neuronal migration and branching was determined recently [28,29]. HDAC6 also modulates cell spreading and motility in non-neuronal cells, like epithelial cells and fibroblasts [30,31]. The acetylation of α-tubulin at K40 by the specific enzyme αTAT1 was

also associated with ciliogenesis and efficient mechanosensation in *Caenorhabditis elegans*, indicating that this post-translational modification is important for axoneme dynamics [32,33]. Even though it is fragmentary, all this information supports the hypothesis of an active participation of acetylation in the dynamics of the axoneme, necessary for differentiation events like the transformation from epimastigotes to infective metacyclic trypomastigotes and from amastigotes to trypomastigotes that occurs in *T. cruzi*. Our results highlight the importance of the bromodomain-containing protein *Tc*BDF3 during these processes. We propose that a protein complex with *Tc*BDF3 could be carrying an enzymatic activity to the flagellum to modify tubulin or other cytoskeletal components. Also, *Tc*BDF3 might carry acetylated α-tubulin from the cell body to the flagellum. However, we cannot rule out the possibility that *Tc*BDF3 sequesters the acetylated lysine residue to protect it from the action of modifying enzymes.

The development of bromodomain inhibitors is a very dynamic and continuously expanding field of research. Several families of small molecules with bromodomain-blocking activity have been described, many of them with potential application against proliferative diseases [15]. Among the seven inhibitors that we assayed against *T. cruzi* epimastigotes, two (I-BET151 and JQ1(+)) showed IC_{50} values lower than 10 μM, and a third (SCG-CBP30) of around 25 μM. The effect of I-BET151 and JQ1(+) over epimastigotes was clearly associated with *Tc*BDF3 inhibition, since both inhibitors interact with the recombinant bromodomain. However, their effect on the parasite cannot be exclusively attributed to *Tc*BDF3 because at least three other bromodomain-containing proteins are present in *T. cruzi*. Among them, we have characterized the nuclear *Tc*BDF2 [34] and recently *Tc*BDF1 [35]. *Tc*BDF2 is a classic histone-binding bromodomain and *Tc*BDF1 is a glycosomal protein that has an important role in infection and amastigote duplication. There is no evidence available yet about the interaction of these bromodomains with the inhibitors. However, we recently showed that a mutated version of *Tc*BDF1 that has no effect on epimastigote growth negatively affects trypomastigote infection and amastigote replication [35]. These results demonstrate that bromodomain factors have different roles during *T. cruzi*'s life cycle. Also, the interaction of I-BET151 with Bdf2 and -3 from *T. brucei* has been recently reported [17]. Although drug repositioning of known bromodomain inhibitors to treat Chagas disease is an interesting strategy, our results suggest that treatment with I-BET151 or JQ1(+) is not optimal due to the rather high IC_{50} values obtained in epimastigotes and apparent low affinity for recombinant *Tc*BDF3. On the other hand, all of the evidence stated strongly supports the fact that bromodomain inhibitors can be considered as potential targets for the development of new drugs against trypanosomiasis and an interesting starting point for rational drug design.

The similarity between the *T. cruzi* BDFs and bromodomains from other organisms is low, with sequence identities always below 20%. Both I-BET151 and JQ1(+) are inhibitors with selectivity for the BET family (which are double bromodomains), but similarity between *T. cruzi* bromodomains and those from the BET family is not evident although *Tc*BDF2 and *Tc*BDF3 can form dimers *in vitro*. In addition, there are other BET inhibitors like PF1 and RVX-208 that did not show activity against *T. cruzi*. *Tc*BDF2 and *Tc*BDF3 show clear substrate selectivity, binding to synthetic acetylated peptides derived from histone H4 and α-tubulin, respectively [16]. Recently, Marchand and Caflisch [30] revised the 26 crystal structures available of 11 different bromodomains, three histones (H4, H3 and H2A), and 16 patterns of acetylation (eight monoacetylation, six diacetylation and two triacetylation). They concluded that in all cases the histone backbone is extended and occupies, in one of the two possible orientations, the bromodomain surface groove lined by the ZA and BC loops. The acetyl-lysine side chain is buried in the cavity between the four helices of the bromodomain, and its oxygen atom accepts hydrogen bonds from a structural water molecule and a conserved asparagine residue in the BC loop. They also observed that the interaction between acetyl-lysine and the bromodomain shows a high degree of symmetry. In parallel to this well-conserved binding motif, they observed a large variety of ancillary interactions suggesting that each bromodomain has a specific binding mode to its substrate. This type of interaction could explain the selectivity of *Tc*BDF2 and *Tc*BDF3 for acetylated histone H4 and α-tubulin. Recently, the crystal structure of *T. brucei* Bdf2 in complex with I-BET151 proved the binding of this molecule to the bromodomain, but showed that the inhibitor has a different binding mode with new interactions not previously reported for human bromodomains [17].

The results presented here show that bromodomain inhibitors can be conceived as a new type of antiparasitic drug. However, in order to better delineate an accurate approach for the development of bromodomain inhibitors as anti-trypanocidal drugs, more research is needed on the function of the other bromodomains.

Materials and methods

Cell culture and infections

Vero cells were cultured in Dulbecco's modified Eagle's medium (DMEM; Gibco, Life Technologies, Carlsbad, CA), supplemented with 2 mM L-glutamine, 10% fetal calf serum (FCS), 100 $U \cdot mL^{-1}$ penicillin and 100 $\mu g \cdot mL^{-1}$ streptomycin.

Metacyclic trypomastigotes were obtained by spontaneous differentiation of epimastigotes at 28 °C. Cell-derived trypomastigotes were obtained by infection with metacyclic trypomastigotes of Vero cell monolayers. After two rounds of infection, the cell-derived trypomastigotes were used for the infection and intracellular amastigote proliferation experiments. Trypomastigotes were collected by centrifugation of the supernatant of previously infected cultures at 2000 ***g*** at room temperature for 10 min and incubated for 3 h at 37 °C in order to allow the trypomastigotes to move from the pellet into the supernatant. After this period, the supernatant was collected and trypomastigotes were counted in a Neubauer chamber. The purified trypomastigotes were preincubated in the presence or absence of 0.25 $\mu g \cdot mL^{-1}$ tetracycline for 3 h and then used to infect new monolayers of Vero cells at a ratio of 10 parasites per cell. After 6 h of infection at 37 °C, the free trypomastigotes were removed by successive washes with phosphate-buffered saline (PBS). Cultures were incubated in complete medium with or without tetracycline (0.25 $\mu g \cdot mL^{-1}$) for 2 days post-infection. Infections were performed in DMEM supplemented with 2% FCS. Cells were then fixed in methanol and the percentage of infected cells and the mean number of amastigotes per infected cell were determined by counting the slides after Giemsa staining using a Nikon Eclipse Ni-U microscope, by counting ~ 1000 cells per slide. The significances of the results were analysed with two-way ANOVA using GRAPHPAD PRISM version 6.0 for Mac (GraphPad Software, La Jolla, CA, USA). Results are expressed as means ± SEM of triplicates, and represent one of three independent experiments performed.

Parasites

Trypanosoma cruzi epimastigotes (Dm28*c* strain) were cultured at 28 °C in liver infusion tryptose (LIT) medium (5 $g \cdot L^{-1}$ liver infusion, 5 $g \cdot L^{-1}$ bacto-tryptose, 68 mM NaCl, 5.3 mM KCl, 22 mM Na_2HPO_4, 0.2% (w/v) glucose and 0.002% (w/v) hemin) supplemented with 10% (v/v) heat-inactivated FCS. Cell viability was assessed by direct microscopic examination. To obtain metacyclic trypomastigotes, epimastigotes were differentiated *in vitro* following the procedure described by Contreras and coworkers under chemically defined conditions using triatomine artificial urine medium (TAU) [3].

Plasmid construction

The *Tc*BDF3 coding sequence was amplified by PCR using BDF3HAFw (5′-AAGGATCC**ATGTATCCGTATGATGTGCCCGGATTATGCT**GGCTCTACGGGT-3′) and BDF3Rv (5′-AACTCGAGCCTCGTCCTCCACCGCC-3′) oligonucleotids. The double mutant (*Tc*BDF3-Y123A/L130A) was constructed using a PCR-based site-directed mutagenesis strategy with the following oligonucleotids: BDF3Y123AFw (5′-CTGCGAGAAGGCTAACGGCG-3′), BDF3Y123ARv (5′-CGCCGTTAGCCTTCTCGCAG-3′), BDF3L130AFw (5′-CGACTCCGCTGCGGTTAAAG-3′) and BDF3L130ARv (5′-CTTTAACCGCAGCGGAGTCG-3′). The restriction sites *Bam*HI and *Xho*I (underlined) were inserted in the oligonucleotides. Proofreading DNA polymerase was used, and DNA purified from cultured *T. cruzi* epimastigotes served as the template. The PCR products were inserted into the pCR 2.1TOPO vector (Invitrogen, Life Technologies, Carlsbad, CA, USA) and sequenced and then inserted into a pENTR3C vector (Gateway System, Invitrogen) and transferred by recombination to p*Tc*INDEX-GW and to pDEST17 (Gateway System, Invitrogen), using LR clonase II enzyme mix (Invitrogen/Life Technologies, Argentina).

Real time PCR (qRT-PCR)

For qRT-PCR primers were designed to amplify a 109 bp fragment of *Tc*BDF3 (5′-TGTTGGCAGATGTGGAGAAGAT-3′ and 5′-CCGCAGCCTTGCCAGTA-3′) and glyceraldehyde 3-phosphate dehydrogenase (GAPDH) (5′-TGGAGCTGCGGTTGTCATT-3′ and 5′-AGCGCGCGTCTAAGACTTACA-3′) as an endogenous control.

TRIzol reagent (Invitrogen) was used to extract total RNA from epimastigotes (5×10^7 cells) and then RNA was treated with RQ1 RNase-free DNaseI (Promega, Madison, WI, USA). First-strand cDNA was synthesized using the First Strand cDNA Synthesis kit (Life Technologies) according to the manufacturer's instructions. The reactions were performed with 500 nM forward and reverse BDF3 primers or 200 nM forward and reverse GAPDH primers, SYBR Green Master Mix (Applied Biosystems, Life Technologies, Argentina) and epimastigote cDNA in triplicates. An ABI PRISM 7000 (Applied Biosystems) thermocycler was used following standard cycling conditions. The data were analysed by the relative stardard curve method normalizing with GAPDH using the 7000 SDS software (Applied Biosystems).

Protein purification

pDEST17-*Tc*BDF3HA and *Tc*BDF3Y123A/L130A-HA were transformed into *Escherichia coli* BL21, and the recombinant proteins (fused to a His tag and haemaglutinin tag) were obtained by induction with 0.1 mM isopropyl-β-D-thiogalactopyranoside overnight at 22 °C. The protein was purified from the inclusion bodies. Briefly, the pellet of the overnight culture

(from 300 to 1000 mL) was washed and resuspended with 10 mM Tris/HCl pH 8 (same volume of the original culture). The cells were ruptured with a high-pressure homogenizer (500 bar once and 1000 bar two more times) and then centrifuged at 16 000 ***g*** for 20 min at 4 °C. The pellet obtained (containing the inclusion bodies) was washed once with distilled water (same volume as the original culture), once with distilled water plus Triton X-100 0.5% (same volume as the original culture), then with distilled water three times (1/10 of the original culture volume). Then the pellet was washed with washing buffer (0.5 M urea, 50 mM NaCl, 0.5 mM EDTA, 10 mM Tris/HCl pH 8) (1/10 of the original culture volume) and finally five times with distilled water (1/10 of the original culture volume). The inclusion bodies were solubilized in 0.1 M glycine–NaOH pH11 overnight at 4 °C with agitation (1/50 of the original culture volume). Then, they were centrifuged at 16 000 ***g*** for 20 min at 4 °C. The solubilized proteins were dialysed against 0.1 M phosphate buffer pH 8. The secondary structure of soluble proteins (5 μM) was measured by circular dicroism spectroscopy using a spectropolarimeter (Jasco J-810, Easton, MD, USA).

Western blot and slot blot

Protein extracts (30–50 μg per well) were separated by SDS/PAGE and transferred to nitrocellulose membranes. The transferred proteins were visualized with Ponceau S. The membranes were treated with 10% non-fat milk in PBS for 2 h and then incubated with specific antibodies diluted in PBS for 3 h. The antibodies used were polyclonal rabbit anti-*Tc*BDF3, monoclonal mouse anti-trypanosome α-tubulin clone TAT-1 (a gift from K. Gull, University of Oxford, UK) and rat monoclonal anti-HA (Roche, Mannheim, Germany). Bound antibodies were detected using peroxidase-labelled anti-mouse, anti-rat or anti-rabbit IgGs (GE Healthcare, Buckinhamshire, UK) and ECL Prime (GE Healthcare) according to the manufacturer's protocol. Slot blot was performed immobilizing 10 μg of synthetic peptides; α-tubulin (PDGAMPSDKTIGVEDDA; Genscript, Piscataway, NJ, USA) and α-tubulin acetylated (ac) on lysine 40 (PDGAMPSDKacTIGVEDDA; Genscript) onto nitrocellulose membranes. The membranes were incubated with recombinant HA-tagged *Tc*BDF3 or *Tc*BDF3Y123A/L130A for 3 h (0.5 $\mu g \cdot mL^{-1}$), and bound proteins were visualized using rat anti-HA antibodies (Roche) and detected as described above. Alternatively, recombinant proteins were preincubated with 10 μM bromodomain inhibitors I-BET151 (donated by GlaxoSmithKline, Stevenage, UK) and JQ1(+) (ApexBio, Houston, TX, USA).

Immunocytolocalization in isolated cytoskeletons and flagellar complexes

The isolated cytoskeletons and flagellar complexes were obtained for immunocytolocalization as previously described by Sasse and Gull [7]. The slides were incubated with the appropriate primary antibodies diluted in 1% BSA in PBS for 3 h at room temperature. Non-bound antibodies were washed with 0.01% Tween 20 in PBS, and then the slides were incubated with fluorescence-conjugated anti-rabbit (Cy3, Invitrogen) and anti-rat (fluorescein, Invitrogen) IgG antibodies and 2 $\mu g \cdot mL^{-1}$ 4,6-diamidino-2-phenylindole (DAPI) for 1 h. The slides were washed with 0.01% Tween 20 in PBS and finally mounted with Vecta-Shield (Vector Laboratories, Burlingame, CA, USA). Images were acquired with a confocal Nikon Eclipse TE-2000-E2 microscope using NIKON EZ-C1 software. ADOBE PHOTOSHOP CS and IMAGEJ software [36] were used to pseudo-colour and process all images.

Transfection of parasites

For inducible expression of wild-type and mutant *Tc*BDF3 in the parasite, we first generated a cell line expressing T7 RNA polymerase and tetracycline repressor genes by transfecting epimastigotes with the plasmid pLew13 using a standard electroporation method. Briefly, epimastigote forms of *T. cruzi* Dm28*c* were grown at 28 °C in LIT medium, supplemented with 10% FCS, to a density of $\sim 3 \times 10^7$ cells per mL. Parasites were then harvested by centrifugation at 2000 ***g*** for 5 min at room temperature, washed once in PBS and resuspended in 0.35 mL of transfection buffer pH 7.5 (0.5 mM $MgCl_2$, 0.1 mM $CaCl_2$ in PBS) to a density of 1×10^8 cells per mL. Cells were then transferred to a 0.2 cm gap cuvette (Bio-Rad Laboratories, Hercucle, CA, USA) and ~ 50 μg of DNA was added in a final volume of 40 μL. The mixture was placed on ice for 15 min and then subjected to two pulses of 450 V and 500 μF using GenePulser II (Bio-Rad Laboratories, Hercules, CA, USA). After electroporation, cells were transferred into 3 mL of LIT medium containing 10% FCS, maintained at room temperature for 15 min and then incubated at 28 °C. After 24 h, Geneticin (G418; Life Technologies) was added at a concentration of 200 $\mu g \cdot mL^{-1}$, and parasites were incubated at 28 °C. After selection, transfected epimastigotes were grown in the presence of 200 $\mu g \cdot mL^{-1}$ of G418. This parental cell line was then transfected with the p*Tc*INDEX-GW constructs and transgenic parasites were obtained after 3 weeks of selection with 100 $\mu g \cdot mL^{-1}$ G418 and 200 $\mu g \cdot mL^{-1}$ Hygromycin B (Sigma-Aldrich, Saint Louis, MO, USA).

Fluorescence spectroscopy

A 2 mL solution containing 5 μM recombinant *Tc*BDF3HA or *Tc*BDF3Y123A/L130A-HA was titrated by successive addition of the bromodomain inhibitors (iBET-152 and JQ1(+)) using concentrations ranging from 0 to 50 μM. Fluorescence spectra were acquired with an excitation wavelength of 295 nm and emission was recorded in the range

of 300–450 nm. All fluorescence measurements were corrected with blank solution and with the emission spectra of each concentration of inhibitor.

Taking into account the inner filter effect in the quenching process, we corrected the fluorescence intensity of *Tc*BDF3 using the following equation [37]: $F_{corr} = F_{obs} \times 10^{(A_{exc}+A_{em})/2}$, where F_{corr} and F_{obs} are the corrected and observed fluorescence intensity of *Tc*BDF3HA, and A_{exc} and A_{em} are the absorption values of the system at the excitation and emission wavelength, respectively.

Treatment with bromodomain inhibitors

To determine the IC_{50} values of the bromodomain inhibitors, epimastigotes of *T. cruzi* Dm28*c* strain were cultured at 28 °C in LIT medium supplemented with 10% FCS in the absence or presence of I-BET151 and JQ1(+) at various concentrations, in triplicate. Cell growth was determined after culture for 72 h by counting viable forms in an automatized haemocytometer adapted to count epimastigotes (WL 19 Counter AA, Weiner Lab, Rosario, Argentina). Then, Dm28*c* wild-type, Dm28*c* p*Tc*INDEXGW-*Tc*BDF3HA and Dm28*c* p*Tc*INDEXGW-*Tc*BDF3Y123A/L130A-HA strains (uninduced and induced with 0.5 $\mu g \cdot mL^{-1}$ tetracycline) were cultured at 28 °C in LIT with FCS in the absence or presence of the bromodomain inhibitors at concentrations above their IC_{50} values.

Statistical analysis

Experiments were performed in triplicate, and at least three independent experiments were performed. Data are presented as the mean ± SEM. Statistical analysis of the data was carried out using two-way ANOVA and unpaired two-tailed Student's *t* test. Differences between the experimental groups were considered significant as follows: $*P < 0.05$, $**P < 0.001$ and $***P < 0.005$. To determine the IC_{50} values, we used nonlinear regression on PRISM 6.0 GRAPHPAD software. Student's *t* test was applied to ascertain the statistical significance of the observed differences in the IC_{50} values.

Acknowledgements

We would like to thank GlaxoSmithKline (GSK) for providing I-BET151 (Trust in Science Collaboration). We are grateful to Israel Gloger, Inmaculada Rioja and Chun-wa Chung from GSK, for their help with the analysis of the results. This work was supported by grants from the 'Agencia Nacional de Ciencia y Tecnología' from Argentina in collaboration with GSK (PICTO2011-0011) and from the 'Consejo Nacional de Investigaciones Científicas y Técnicas' (CONICET, PIP2010-0685) from Argentina. We would like to thank Dolores Campos and Romina Manarin for their technical assistance with cell and parasites culture. Also special thanks to Rodrigo Vena for the assistance in the acquisition of confocal images.

Author contributions

VLA, PC, CR and EC planned the experiments, VA, CR and PC performed the experiments, and VLA, JAC and EC analysed the data and wrote the paper.

References

1 WHO (2012) Research Priorities for Chagas Disease, Human African Trypanosomiasis and Leishmaniasis. World Health Organization Press, Geneva, Switzerland.
2 De Souza W, De Carvalho TMU & Barrias ES (2010) Review on *Trypanosoma cruzi*: host cell interaction. *Int J Cell Biol* **2010**, doi: 10.1155/2010/295394.
3 Contreras VT, Araujo-Jorge TC, Bonaldo MC, Thomaz N, Barbosa HS, Meirelles Mde N & Goldenberg S (1988) Biological aspects of the Dm 28c clone of *Trypanosoma cruzi* after metacyclogenesis in chemically defined media. *Mem Inst Oswaldo Cruz* **83**, 123–133.
4 Schneider A, Plessmann U & Weber K (1997) Subpellicular and flagellar microtubules of *Trypanosoma brucei* are extensively glutamylated. *J Cell Sci* **110** (Pt 4), 431–437.
5 Kohl L & Gull K (1998) Molecular architecture of the trypanosome cytoskeleton. *Mol Biochem Parasitol* **93**, 1–9.
6 Souto-Padron T, Cunha e Silva NL & de Souza W (1993) Acetylated alpha-tubulin in *Trypanosoma cruzi*: immunocytochemical localization. *Mem Inst Oswaldo Cruz* **88**, 517–528.
7 Sasse R & Gull K (1988) Tubulin post-translational modifications and the construction of microtubular organelles in *Trypanosoma brucei*. *J Cell Sci* **90** (Pt 4), 577–589.
8 L'Hernault SW & Rosenbaum JL (1985) Chlamydomonas alpha-tubulin is posttranslationally modified by acetylation on the epsilon-amino group of a lysine. *Biochemistry* **24**, 473–478.
9 Soppina V, Herbstman JF, Skiniotis G & Verhey KJ (2012) Luminal localization of α-tubulin K40 acetylation by cryo-EM analysis of fab-labeled microtubules. *PLoS ONE* **7**, e48204.
10 Szyk A, Deaconescu AM, Spector J, Goodman B, Valenstein ML, Ziolkowska NE, Kormendi V, Grigorieff N & Roll-Mecak A (2014) Molecular basis for age-dependent microtubule acetylation by tubulin acetyltransferase. *Cell* **157**, 1405–1415.
11 Filippakopoulos P & Knapp S (2012) The bromodomain interaction module. *FEBS Lett* **586**, 2692–2704.

12 Burton PR (1984) Luminal material in microtubules of frog olfactory axons: structure and distribution. *J Cell Biol* **99**, 520–528.
13 Garvalov BK, Zuber B, Bouchet-Marquis C, Kudryashev M, Gruska M, Beck M, Leis A, Frischknecht F, Bradke F, Baumeister W *et al.* (2006) Luminal particles within cellular microtubules. *J Cell Biol* **174**, 759–765.
14 Bouchet-Marquis C, Zuber B, Glynn A-M, Eltsov M, Grabenbauer M, Goldie KN, Thomas D, Frangakis AS, Dubochet J & Chrétien D (2007) Visualization of cell microtubules in their native state. *Biol Cell* **99**, 45–53.
15 Hewings DS, Rooney TPC, Jennings LE, Hay DA, Schofield CJ, Brennan PE, Knapp S & Conway SJ (2012) Progress in the development and application of small molecule inhibitors of bromodomain-acetyl-lysine interactions. *J Med Chem* **55**, 9393–9413.
16 Alonso VL, Villanova GV, Ritagliati C, Machado Motta MC, Cribb P & Serra EC (2014) *Trypanosoma cruzi* bromodomain factor 3 (TcBDF3) binds acetylated α tubulin and concentrates in the flagellum during metacyclogenesis. *Eukaryot Cell* **13**, 822–831.
17 Schulz D, Mugnier MR, Paulsen E-M, Kim H-S, Chung CW, Tough DF, Rioja I, Prinjha RK, Papavasiliou FN & Debler EW (2015) Bromodomain proteins contribute to maintenance of bloodstream form stage Identity in the African trypanosome. *PLoS Biol* **13**, e1002316.
18 Alonso VL, Ritagliati C, Cribb P & Serra EC (2014) Construction of three new Gateway ® expression plasmids for *Trypanosoma cruzi*. *Mem Inst Oswaldo Cruz* **109**, 1081–1085.
19 Mirguet O, Lamotte Y, Donche F, Toum J, Gellibert F, Bouillot A, Gosmini R, Nguyen V-L, Delannée D, Seal J *et al.* (2012) From ApoA1 upregulation to BET family bromodomain inhibition: discovery of I-BET151. *Bioorg Med Chem Lett* **22**, 2963–2967.
20 Filippakopoulos P, Qi J, Picaud S, Shen Y, Smith WB, Fedorov O, Morse EM, Keates T, Hickman TT, Felletar I *et al.* (2010) Selective inhibition of BET bromodomains. *Nature* **468**, 1067–1073.
21 Dhalluin C, Carlson JE, Zeng L, He C, Aggarwal K & Zhou MM (1999) Structure and ligand of a histone acetyltransferase bromodomain. *Nature* **399**, 491–496.
22 Ritagliati C, Alonso VL, Manarin R, Cribb P & Serra EC (2015) Overexpression of cytoplasmic TcSIR2RP1 and mitochondrial TcSIR2RP3 impacts on *Trypanosoma cruzi* growth and cell invasion. *PLoS Negl Trop Dis* **9**, e0003725.
23 Ferreira LR, Dossin Fde M, Ramos TC, Freymüller E & Schenkman S (2008) Active transcription and ultrastructural changes during *Trypanosoma cruzi* metacyclogenesis. *An Acad Bras Cienc* **80**, 157–166.
24 Seal J, Lamotte Y, Donche FF, Bouillot A, Mirguet O, Gellibert FF, Nicodeme E, Krysa G, Kirilovsky J, Beinke S *et al.* (2012) Identification of a novel series of BET family bromodomain inhibitors: binding mode and profile of I-BET151 (GSK1210151A). *Bioorg Med Chem Lett* **22**, 2968–2972.
25 Jung M, Philpott M, Müller S, Schulze J, Badock V, Eberspächer U, Moosmayer D, Bader B, Schmees N, Fernández-Montalván A *et al.* (2014) Affinity map of bromodomain protein 4 (BRD4) interactions with the histone H4 tail and the small molecule inhibitor JQ1. *J Biol Chem* **289**, 9304–9319.
26 Black MM, Baas PW & Humphries S (1989) Dynamics of alpha-tubulin deacetylation in intact neurons. *J Neurosci* **9**, 358–368.
27 Falconer MM, Vielkind U & Brown DL (1989) Association of acetylated microtubules, vimentin intermediate filaments, and MAP 2 during early neural differentiation in EC cell culture. *Biochem Cell Biol* **67**, 537–544.
28 Creppe C, Malinouskaya L, Volvert ML, Gillard M, Close P, Malaise O, Laguesse S, Cornez I, Rahmouni S, Ormenese S *et al.* (2009) Elongator controls the migration and differentiation of cortical neurons through acetylation of alpha-tubulin. *Cell* **136**, 551–564.
29 Conacci-Sorrell M, Ngouenet C & Eisenman RN (2010) Myc-nick: a cytoplasmic cleavage product of Myc that promotes alpha-tubulin acetylation and cell differentiation. *Cell* **142**, 480–493.
30 Birdsey GM, Dryden NH, Shah AV, Hannah R, Hall MD, Haskard DO, Parsons M, Mason JC, Zvelebil M, Gottgens B *et al.* (2012) The transcription factor Erg regulates expression of histone deacetylase 6 and multiple pathways involved in endothelial cell migration and angiogenesis. *Blood* **119**, 894–903.
31 Lafarga V, Mayor F & Penela P (2012) The interplay between G protein-coupled receptor kinase 2 (GRK2) and histone deacetylase 6 (HDAC6) at the crossroads of epithelial cell motility. *Cell Adh Migr* **6**, 495–501.
32 Shida T, Cueva JG, Xu Z, Goodman MB & Nachury MV (2010) The major alpha-tubulin K40 acetyltransferase alphaTAT1 promotes rapid ciliogenesis and efficient mechanosensation. *Proc Natl Acad Sci USA* **107**, 21517–21522.
33 Akella JS, Wloga D, Kim J, Starostina NG, Lyons-Abbott S, Morrissette NS, Dougan ST, Kipreos ET & Gaertig J (2010) MEC-17 is an alpha-tubulin acetyltransferase. *Nature* **467**, 218–222.
34 Villanova GV, Nardelli SC, Cribb P, Magdaleno A, Silber AM, Motta MC, Schenkman S & Serra E (2009) Trypanosoma cruzi bromodomain factor 2 (BDF2) binds to acetylated histones and is accumulated after UV irradiation. *Int J Parasitol* **39**, 665–673.
35 Ritagliati C, Villanova GV, Alonso VL, Zuma AA, Cribb P, Motta MCM & Serra EC (2015) Glycosomal

bromodomain factor 1 from *Trypanosoma cruzi* enhances trypomastigotes cell infection and intracellular amastigotes growth. *Biochem J* **473**, 73–85.
36 Collins TJ (2007) ImageJ for microscopy. *Biotechniques* **43**, 25–30.
37 Samworth CM, Degli Esposti M & Lenaz G (1988) Quenching of the intrinsic tryptophan fluorescence of mitochondrial ubiquinol–cytochrome-c reductase by the binding of ubiquinone. *Eur J Biochem* **171**, 81–86.